calculated using the modified $k-\epsilon$ model.[1] The measurements clearly agree well with the predicted values. The concentration gradients generally were correctly predicted in the forward part of the recirculation zone and somewhat underpredicted past reattachment. Downstream of reattachment, the main and bleed gases, thus, were slightly better mixed than predicted. Closer to the step, the process was more diffusion-controlled. This observation is in close agreement with the expectations from the velocity measurements.[1] Furthermore, the mean concentration data obtained using the more sophisticated deconvolution are not significantly different from those obtained with the simple data reduction technique.[2]

The real power of this improved technique, however, becomes evident when calculating the velocity-concentration covariances, which could not be obtained at all using the simplified data reduction scheme. Figure 2 shows the profiles of the velocity-concentration covariances at the same locations in the test section as in the previous example. Once again, the predicted values are shown as a solid line. Clearly, the agreement between the measured and calculated values of the covariance is not as good as those for the mean concentrations. In part, this could be due to remaining uncertainties in the measured values of the covariance. However, Fig. 2b, which corresponds to the reattachment location, indicates acceptable reproducibility of the data, especially considering the low signal-to-noise ratio of the measurements. Therefore, it appears that whereas the model quite accurately predicts the overall shape of the covariance profiles, it consistently overpredicts the magnitude of the covariance.

Conclusions

Molecular mixing in the recirculation zone, behind a backward-facing step with bleed, was found to be excellent. Agreement between the measured bleed gas concentration profiles and those predicted using a modified $k-\epsilon$ model were very good, although the flow downstream of recirculation was found to be better mixed than predicted. An improved data reduction technique for removing background noise really showed its full potential in the extraction of the velocity concentration covariance. Despite the remaining uncertainties in the covariance, it becomes clear that the $k-\epsilon$ model, while correctly calculating the shape of the profile, tends to overpredict the magnitude of the velocity-concentration covariance.

Acknowledgment

This work was supported by the Air Force Office of Scientific Research under Grant AFOSR-83-0356. The authors wish to thank Dr. W. C. Strahle for developing the data reduction technique and for his extensive contributions to this work. Thanks also to Dr. R. Latham for his help in coding the data acquisition software.

References

[1]Richardson, J., de Groot, W. A., Jagoda, J. I., Walterick, R. E., Hubbartt, J. E., and Strahle, W. C., *Journal of Propulsion and Power,* Vol. 1, No. 6, Nov.-Dec. 1985, pp. 488-493.

[2]de Groot, W. A., Latham, R., Jagoda, J. I., and Strahle, W. C., *AIAA Journal,* Vol. 25, Aug. 1987, pp. 1142-1144.

[3]Walterick, R. E., de Groot, W. A., Jagoda, J. I., and Strahle, W. C., AIAA Paper 88-0052, Jan. 1988.

[4]Penney, C. M., *Journal of the Optical Society of America,* Vol. 59, Jan. 1969, pp. 34-38.

[5]Driscoll, J. F., Schefer, R. W., and Dibble, R. W., "Mass Fluxes $\rho' u''$ and $\rho' v''$ Measured in a Turbulent Nonpremixed Flame," *Proceedings of the 19th International Symposium on Combustion,* The Combustion Inst., Pittsburgh, PA, 1982, pp. 477-485.

[6]Schefer, R. W. and Dibble, R. W., *AIAA Journal,* Vol. 23, July 1985, pp. 1070-1078.

[7]Strahle, W. C. and de Groot, W. A., "Extraction of Useful Data from Noise Contaminated PDF's," *Combustion and Flame* (to be published).

Diagonal Implicit Multigrid Calculation of Inlet Flowfields

D. A. Caughey* and R. K. Iyer†
Cornell University, Ithaca, New York

I. Introduction

A DIAGONAL implicit multigrid algorithm to solve the Euler equations has been applied by Caughey[1] to compute the transonic flow past a two-dimensional airfoil. It is the purpose of this Note to describe an extension of that algorithm to compute the supersonic flow past and within a two-dimensional planar inlet.

II. Analysis

Inviscid compressible flows are governed by the Euler equations, which are written in conservation form in order to capture shocks correctly. The integral form of the conservation laws is

$$\frac{\partial}{\partial t}\iint_S w\,dx\,dy + \int_{\partial S}(f\,dy - g\,dx) = 0 \tag{1}$$

where w is the vector of flow variables and f,g are the flux vectors in the x and y coordinate directions. The integration is over the region S with boundary ∂S. In the present discretization, which is based on that of Jameson et al.,[2] the temporal and spatial approximations are kept separate. This decoupling ensures a steady-state solution that is independent of the time step with which the solution is advanced from some initial condition. The spatial discretization is performed using a finite-volume approximation, which consists in applying the integral form of the conservation laws as defined by Eq. (1) to each quadrilateral cell in the physical domain. In the present calculation, the flow variables are taken to represent the average values for each mesh cell. The values required for the evaluation of the fluxes in Eq. (1) are taken to be constant on each face, and equal to the simple average of the values corresponding to the cells which share the face. This formulation is equivalent to a centered difference scheme that is second-order accurate in the mesh spacing in the physical domain when the mesh is smooth.

The use of centered differences has the drawback of allowing the solution to decouple at odd- and even-numbered points and of allowing oscillations in the solution near shock waves. To counter these effects, following Jameson et al.,[2] a blend of second- and fourth-difference artificial dissipation terms is added to the equations. The difference approximation, including dissipation terms, can be written in the form

$$\frac{dW_{i,j}}{dt} + Qw_{i,j} - Dw_{i,j} = 0 \tag{2}$$

where Q and D are, respectively, the operators representing the spatial discretization of the flux terms and the dissipative terms. The artificial dissipation is constructed such that simultaneously the second-difference terms are activated and the fourth-difference terms are switched off near shock waves, allowing them to be captured with little or no overshoot. The normalized second-difference of the pressure

$$\nu_{i,j} = \frac{|p_{i+1,j} - 2p_{i,j} + p_{i-1,j}|}{p_{i+1,j} + 2p_{i,j} + p_{i-1,j}}$$

is used to modulate these dissipative terms.

Received Feb. 29, 1988; revision received April 27, 1988.

*Professor, Sibley School of Mechanical and Aerospace Engineering. Associate Fellow AIAA.

†Graduate Research Assistant, Sibley School of Mechanical and Aerospace Engineering.

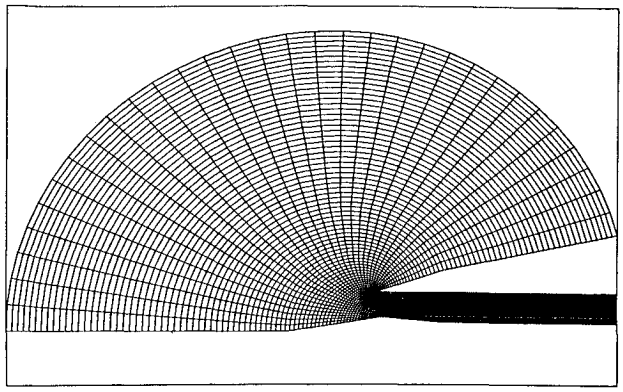

Fig. 1 Grid around and within two-dimensional planar inlet. Grid shown has 128 × 32 cells in wraparound and body-normal directions, respectively.

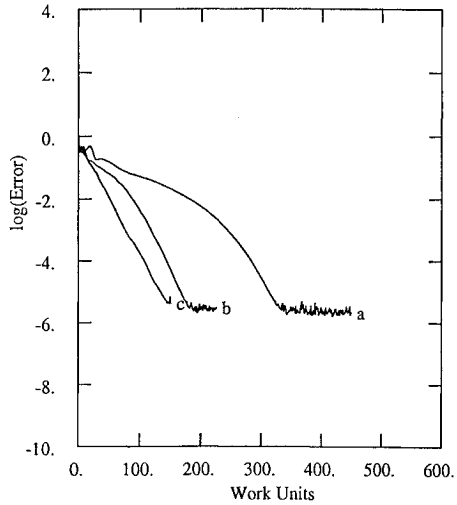

Fig. 2 Convergence histories for calculation of flow through planar inlet. Average residual is plotted vs work units for a) single-grid calculation; b) two-level multigrid calculation; and c) four-level multigrid calculation.

Following Chaussee and Pulliam,[3] a diagonal alternating direction implicit (ADI) time-stepping scheme is used in this study. Let A and B be defined as the Jacobians of the flux vectors in the two directions in the computational domain. These matrices are diagonalized using the similarity transformations

$$\Lambda_A = Q_A^{-1} A Q_A, \qquad \Lambda_B = Q_B^{-1} B Q_B$$

where the columns of Q_A and Q_B are, respectively, the eigenvectors of A and B, and Λ_A and Λ_B are diagonal matrices. Introducing the diagonalization procedure into the implicit operator obtained using an approximate-factorization ADI scheme enables the time-stepping scheme to be written in the form

$$\{I + \theta\Delta t[\Lambda_{A_{i,j}^n}\delta_\xi - \epsilon_{i,j}^{(2)}\delta_\xi^2(1/h) + \epsilon_{i,j}^{(4)}\delta_\xi^4(1/h)]\}Q_{A_{i,j}^n}^{-1}Q_{B_{i,j}^n}$$

$$\{I + \theta\Delta t[\Lambda_{B_{i,j}^n}\delta_\eta - \epsilon_{i,j}^{(2)}\delta_\eta^2(1/h) + \epsilon_{i,j}^{(4)}\delta_\eta^4(1/h)]\}\Delta V_{i,j}^n = Q_{A_{i,j}^n}^{-1}R_{i,j} \tag{3}$$

where

$$\Delta W_{i,j}^n = Q_{B_{i,j}^n}\Delta V_{i,j}^n \tag{4}$$

is the correction to be added to the solution vector in each cell at the nth time step. Equation (3) is solved in two steps. First, intermediate corrections are computed by solving a system of four scalar pentadiagonal systems along each ξ line. These intermediate corrections are then used to compute the final corrections by the solution of four scalar pentadiagonal systems along each η line.

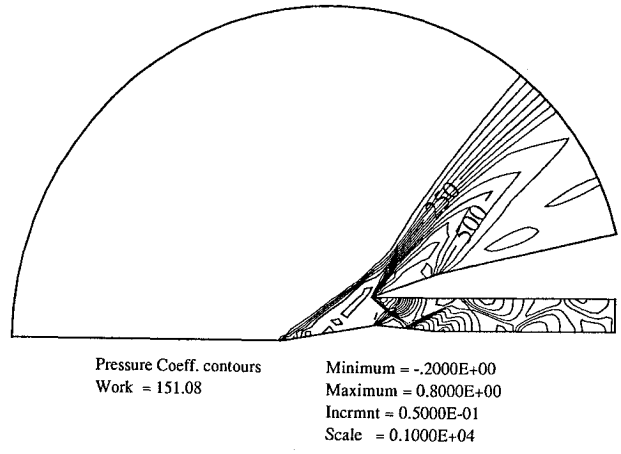

Fig. 3 Contours of constant pressure for computed flow at freestream Mach number $M_\infty = 2$ through planar inlet. Contour labels are 1000 times pressure coefficient.

The multigrid method of Jameson[4] is incorporated to increase computational efficiency. A sequence of grids, ranging from very fine to very coarse, is used so that the error in any wave-number band is eliminated on a suitable grid. High wave-number errors on each grid are efficiently eliminated using the basic time-stepping scheme. In order to remove rapidly the low wave-number errors (which are effectively high wave-number errors on a suitably coarse mesh), smoothing operations are performed on successively coarser meshes. As the mesh becomes coarser, the computational work required to perform the smoothing becomes proportionally less also.

III. Results

The inlet studied here has a 10-deg ramp and a 20-deg wedge cowl. A 128 × 32 cell, body-fitted grid was generated around and within the inlet using a slight modification of the conformal mapping method of Caughey and Jameson.[5] (See Fig. 1). The mesh point with the largest ordinate is taken as the dividing point between inflow and outflow on the circular far-field boundary. The test case presented here is a supersonic flow at a freestream Mach number $M_\infty = 2$. Because the flow in the farfield is supersonic, all flow variables are specified at points on the inflow boundary, while all flow variables are extrapolated from the interior of the domain at points on the outflow boundary. Figure 2 illustrates the acceleration in convergence to steady state achieved by the multigrid method. The curves represent the average over all cells in the field of $|\Delta\rho/\Delta t|$ (the residual of the continuity equation) as a function of computational work, measured in work units; one work unit is equivalent to the CPU time required for a single time step on the fine grid. The labeled curves represent the convergence of the scheme applied a) on a single grid, b) using two levels of multigrid, and c) using four levels of multigrid, respectively. Note that the four-grid level calculation converges more than 2.5 times faster than the single-grid calculation. Although the improvement is significant, it is not as large as would be expected for transonic or subsonic flows, since even explicit time stepping is reasonably efficient for flows that are entirely supersonic. Contours of constant pressure for the steady-state solution are presented in Fig. 3. The interaction between expansion waves and shock waves inside the inlet channel is successfully captured. Figures 4 and 5 show the pressure distributions on the centerbody and cowl inner surfaces, respectively. These results are in reasonable agreement with results obtained by Chaussee and Pulliam,[3] who performed similar calculations on an identical inlet. Note, however, that the capture of the reflected wave system as one moves downstream in the channel is somewhat sharper in the present results. This is probably due both to the slightly finer grid used in the present study and to the introduction of less spurious dissipation by the present scheme. Chaussee and Pulliam reported achieving convergence in 800 iterations for a 66 × 36 grid. For the results presented

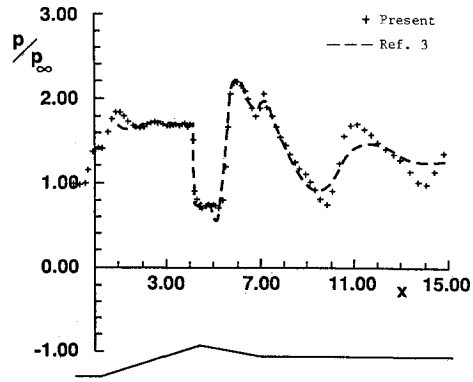

Fig. 4 Pressure distributions computed on inlet centerbody. Symbols represent present solution; broken lines represent solution of Ref. 3.

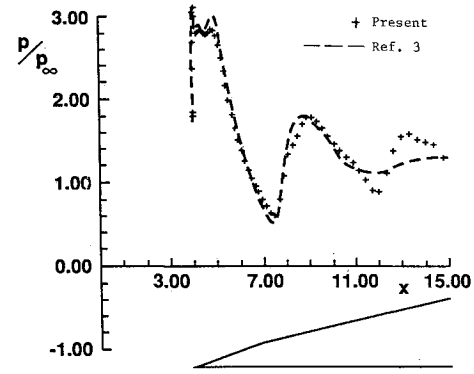

Fig. 5 Pressure distributions computed on cowl inner surface. Symbols represent present solution; broken lines represent solution of Ref. 3.

here, the incorporation of multigrid enables convergence to the steady state in the equivalent of 125 iterations for the four-grid level calculation.

References

[1]Caughey, D. A., "A Diagonal Implicit Multigrid Algorithm for the Euler Equations," *AIAA Journal,* Vol. 26, July 1988, pp. 841-851.

[2]Jameson, A., Schmidt, W., and Turkel, E., "Numerical Solution of the Euler Equations by Finite-Volume Methods Using Runge-Kutta Time-Stepping Schemes," AIAA Paper 81-1259, June 1981.

[3]Chaussee, D. S. and Pulliam, T. H., "Two-Dimensional Inlet Simulation Using a Diagonal Implicit Algorithm," *AIAA Journal,* Vol. 19, Feb. 1981, pp. 153-159.

[4]Jameson, A., "Multigrid Solution of the Euler Equations," Mechanical and Aerospace Engineering, Princeton Univ., Princeton, NJ, MAE Rept. 1316, June 1983.

[5]Caughey, D. A. and Jameson, A., "Accelerated Iterative Calculation of Transonic Nacelle Flow Fields," *AIAA Journal,* Vol. 15, Oct. 1977, pp. 1474-1480.

Görtler Instability of Wall Jets

J. M. Floryan*
University of Western Ontario, London, Ontario, Canada

Introduction

IT has recently been shown by Floryan[1] that Görtler instability might occur over concave as well as convex walls, provided that the velocity distribution inside the boundary layer violates the inviscid stability criterion.[1] It has also been suggested[1] that when velocity distribution is nonmonotonic, the flow will consist of layers that alternatively violate and satisfy the stability criterion, and this could lead to an interesting evolution of the unstable motion. The purpose of this Note is to analyze the stability of a simplest flow of this type, i.e., a wall jet over a concave surface, which consists of an inviscidly unstable layer located next to the wall and an inviscidly stable layer located farther away. The appropriate velocity field is described by Glauert.[2] The required disturbance equations and the method of solution are described in Ref. 3. The same problem has been considered by Kahawita;[4] however, the present analysis, which is much more extensive, is based on a model rationally incorporating the effects of boundary-layer growth[3] and, therefore, the present results represent a considerable improvement over the results of Ref. 4.

Results

The disturbance growth process[5] is illustrated in Figs. 1-6. Figure 1 displays curves of constant spatial amplification rate β as a function of the spanwise wave number α and the Görtler number $G = U_\infty \delta_r/\nu\ (\delta_r/R)^{1/2}$ (where R denotes the radius of curvature of the wall). The wall-jet thickness, $\delta_r = (\nu\tilde{\Phi}/U_\infty)^{1/2}$, is the length scale, where U_∞ is the maximum of the streamwise velocity component of the jet, ν the kinematic viscosity, and $\tilde{\Phi}$ the distance from the virtual origin of the jet. The neutral curve corresponds to $\beta = 0$, and its minimum occurs for $\alpha \to 0$; the critical value of the Görtler number is $G_c \approx 1.0$. Because there is no critical wave number, the wavelength selection mechanism is determined by the disturbance growth process. It is convenient to introduce a dimensionless wavelength parameter $\Lambda = F^{1/3} \lambda^{1/3} \nu^{-1} (\lambda/R)^{1/2}$ (which is constant in the flow direction) in order to follow streamwise development of a vortex of a constant dimensional wavelength λ (dimensionless wave number α changes in the flow direction because of variations of the length scale δ_r). Here F is the dimensional "flux of external momentum flux."[2] Straight lines with slope 5/6 correspond to constant Λ in Fig. 1. One might presume that the vortex described by Λ that stays closest to the line of maximum amplification in Fig. 1 has the most favorable conditions to grow. Figure 2 displays the total amplification of disturbances that occurred between the neutral curve and streamwise locations

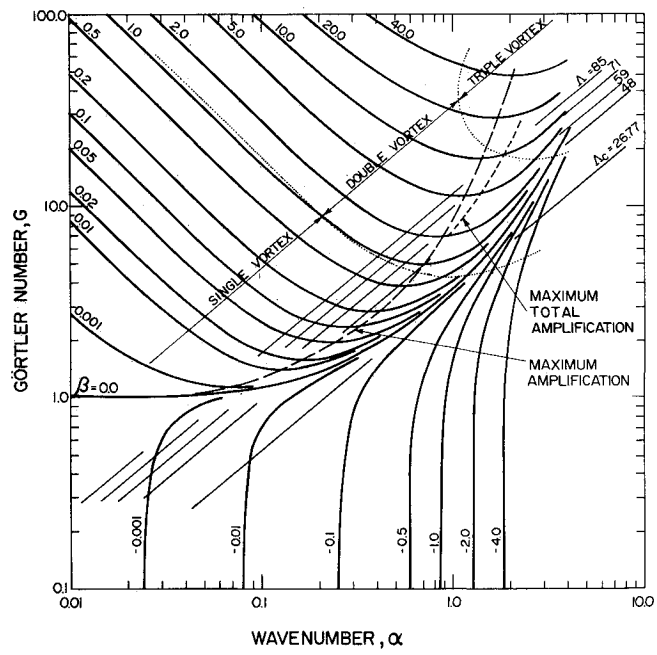

Fig. 1 Curves of constant amplification rate β as a function of Görtler number G and wave number α for the first mode of the Görtler instability of wall jets over a concave wall.

Received July 28, 1987.

*Associate Professor, Department of Mechanical Engineering.